EGG-CDD-6054

September 1982

PDR

ADVANCED DEFORMATION MODELS FOR FRAP-T6

V. N. Shah
E. R. Carlson
G. A. Berna

Idaho National Engineering Laboratory
Operated by the U.S. Department of Energy

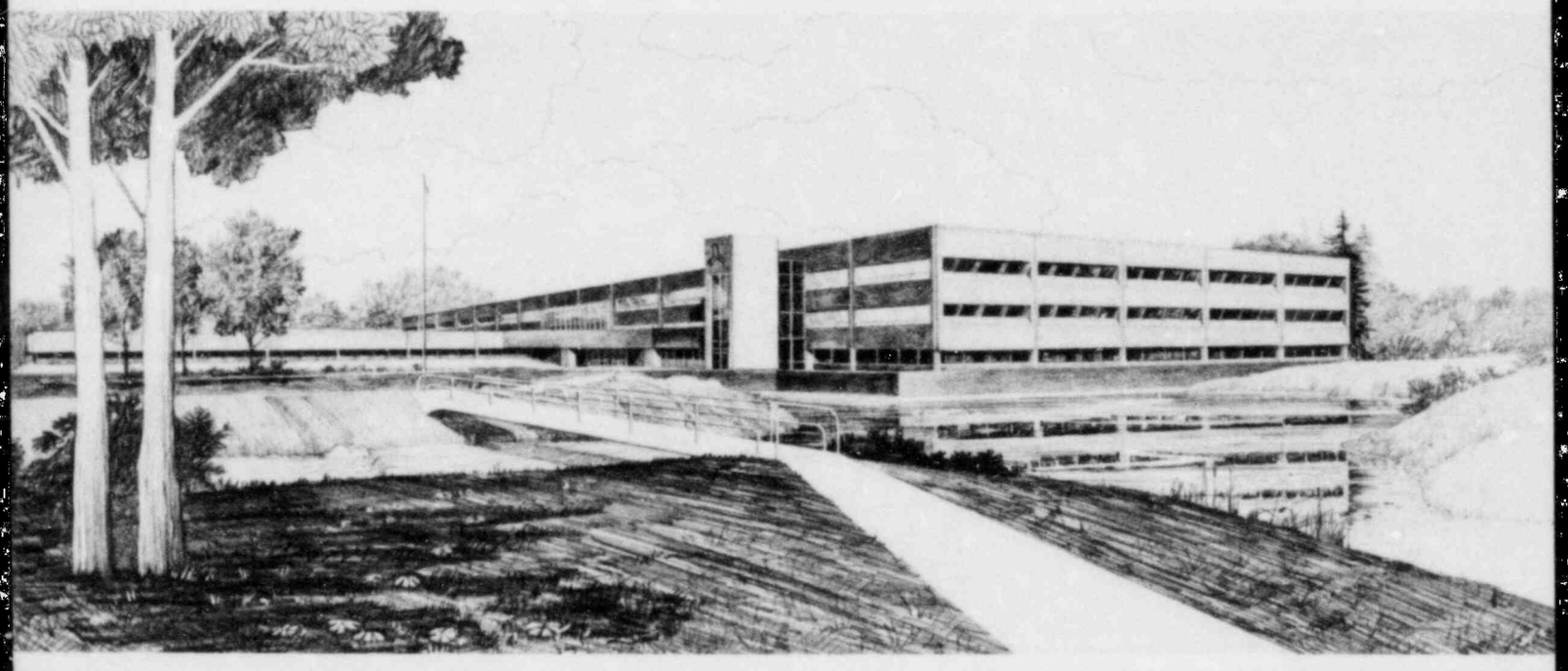

This is an informal report intended for use as a preliminary or working document

Prepared for the
U.S. NUCLEAR REGULATORY COMMISSION
Under DOE Contract No. DE-AC07-76ID01570
Fin. No. A6050

EG&G Idaho

EG&G Idaho, Inc.

FORM EG&G-398
(Rev. 11-79)

INTERIM REPORT

Accession No. _____

Report No. EGG-CDD-6054

Contract Program or Project Title: Fuel Behavior Model Development Program

Subject of this Document: Advanced Deformation Models for FRAP-T6

Type of Document: Internal Report

Author(s): V. N. Shah
E. R. Carlson
G. A. Berna

Date of Document:

Responsible NRC Individual and NRC Office or Division: G. P. Marino, NRC-RES

This document was prepared primarily for preliminary or internal use. It has not received full review and approval. Since there may be substantive changes, this document should not be considered final.

EG&G Idaho, Inc.
Idaho Falls, Idaho **83415**

Prepared for the
U.S. Nuclear Regulatory Commission
Washington, D.C.
Under DOE Contract No. **DE-AC07-76ID01570**
NRC FIN No. A6050

INTERIM REPORT

ABSTRACT

This report describes the advanced deformation models implemented in the FRACAS-II fuel rod mechanics analysis subcode used with the FRAPCON-2 and FRAP-T6 computer codes. The models included are a trapped-fuel stack model, an early axial pellet cladding mechanical interaction model, and a burnup and power dependent fuel relocation model. The objective of this work was to improve FRACAS-II stress-strain modeling capability under PCMI conditions. The updated FRACAS-II subcode was incorporated in FRAP-T6 and calculations made for experimental rods in Halden and PBF. The calculations were compared with experimental data. With the advanced models, the FRAP-T6 mechanics calculations were improved.

SUMMARY

Advanced deformation models were added to the FRAP-T6 computer code to enhance the mechanical modeling during PCMI. The models which were added include an early axial pellet cladding mechanical interaction (PCMI) model, a trapped-fuel stack model, and a burnup and power dependent fuel relocation model. After incorporating these models into FRAP-T6, acceptance tests were conducted using experimental data from IFA-508 to assure that the models were properly incorporated and that they function as intended. The results of these tests were that the models function properly and have improved the mechanical calculations in areas identified as deficient during a development assessment of FRACAS-II performed earlier. The acceptance tests, however, point to the need for three additional models needed to complete the FRACAS-II mechanics package. It is concluded that a fuel-cladding slippage model, a fuel creep model, and a relocation relaxation model should be incorporated into FRAP-T6. The latter two models are developed and ready for incorporation into FRAP-T6, but data must be gathered to develop an empirical model for slippage between fuel and cladding.

CONTENTS

FIGURES

TABLES

ADVANCED DEFORMATION MODELS FOR FRAP-T6

1. INTRODUCTION

The capability to accurately calculate the performance of light water reactor (LWR) fuel rods under transient and hypothetical accident conditions is a major objective of the Nuclear Regulatory Commission's (NRC) Water Reactor Safety Program. To achieve this objective, NRC is sponsoring development of the FRAPCON-2[1] (Fuel Rod Analysis Program--Steady State) and FRAP-T6[2] (Fuel Rod ANalysis Program--Transient) computer codes. FRAPCON-2 calculates the steady state response of a LWR fuel rod during long term burnup. FRAP-T6 calculates the transient response of a LWR fuel rod during operational transients and hypothetical accidents such as a power-cooling mismatch or a loos-of-coolant accident. Both codes have a mechanics model (FRACAS-II[3]) to calculate elastic-plastic cladding and fuel deformations. The objective of fRACAS-II is to provide a mechanistically based model that calculates the interrelateddeformation of fuel and cladding.

The developmental assessment of the FRACAS-II model showed that some of the basic mechanical models needed to calculate fuel rod performance were either incorrect or missing, and therefore the FRACAS-II model was not acceptable for reliably determining the extent of cladding damage and ultimately cladding failure.[4] Based on the recommendations made during the assessment of the FRACAS-II model, three new mechanical models were developed and incorporated in FRACAS-II.

The first model initiates an axial PCMI at lower power than is needed for radial PCMI. This phenomena of early axial PCMI is exhibited by test results as shown in Figure 1. The axial PCMI starts at 15 kW/m while radial PCMI starts at about 29 kW/m. The second model analyzes the trapped-stack condition in the fuel rod. This is a mechanistic model and is needed for the accurate calculation of cladding strains when the axial power profile is not uniform. The third model calculates the fuel relocation due to cracking. This is an empirical model based on test results.[5] It calculates relocation as a function of cold gap, power and burnup. The previous relocation model in FRACAS-II was only a function of cold gap.

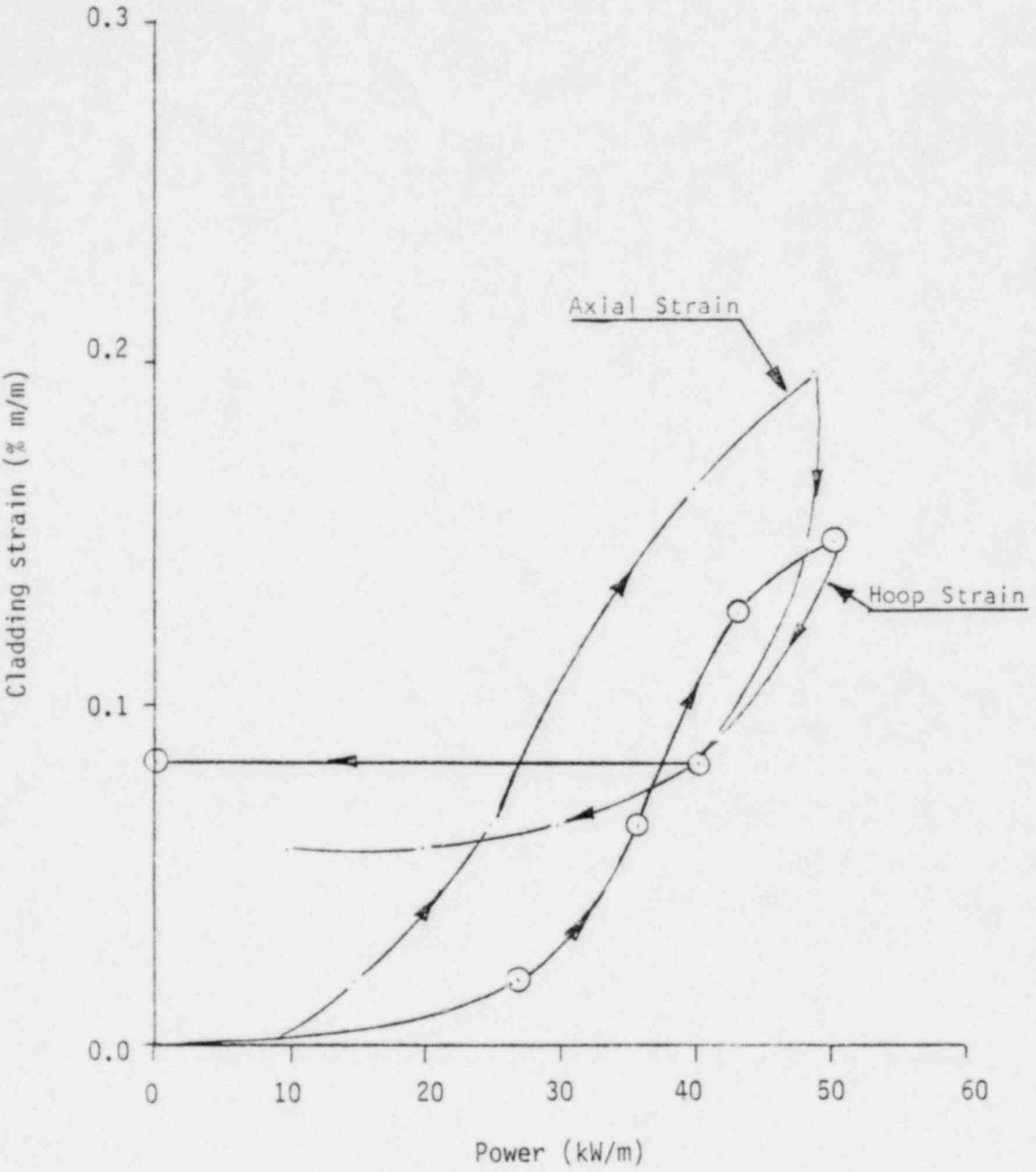

Figure 1. Measured cladding strains versus linear heat rating in Rod 11 during initial power cycle.

Section 2 presents the descriptions of the newly added models. Section 3 presents a description of the coding and its implementation. Section 4 presents the results of acceptance testing and gives recommendations.

2. MODEL DESCRIPTION

Three advanced models for the fuel rod deformation are reported here. The first two models are mechanicistically based while the third model is based on empirical relations.

The early axial PCMI model is described first. Then the trapped-stack model and fuel relocation model are described.

2.1 Early Axial PCMI Model

Axial PCMI requires few contact points to establish firm axial contact between cladding and pellet, while radial PCMI requires contact between cladding and pellet around the complete circumference. Axial PCMI starts at lower power than radial PCMI for several reasons: random pellet stacking, pellet cocking or misalignment, cladding ovality, cladding eccentricity, pellet chipping, grid pinching of cladding, and/or pellet hourglassing. A simple model is developed to address this phenomena. This model initiates axial PCMI earlier than the radial PCMI during increasing power and ceases radial PCMI prior to ceasing of axial PCMI during decreasing power. This model assumes that the axial PCMI begins when the radial gap between cladding and fuel is less than the locking gap.[6] The locking gap is determined from experimental results for cladding hoop and axial strains during a power cycle.

Initially the randomly stacked pellets are in partial contact with the cladding tube at several points along the fuel rod. The radial frictional forces between adjacent pellets and axial frictional forces between pellets and cladding at the contact points introduce an axial force in the pellet column. The axial force increases as the distance from the upper end of the pellet column increases and it is an exponential function of the number of contact points.[7] During the first power ramp, most of the original eccentricity is removed in the upper part of the rod, whereas considerable eccentricity is preserved in the lower part of the fuel column which has higher axial force and thus, higher frictional forces. In the subsequent

power cycles, axial PCMI and radial PCMI will begin at approximately the same power in the upper part of the rod, while axial PCMI will begin at a lower power than for radial PCMI in the lower part of the rod until all the eccentricity is removed.[7]

A model is developed to account for sliding along the axial direction in the fuel rod. The pellet column experiences larger thermal expansion than the cladding during operation. For several reasons, all the excessive axial thermal expansion of the pellet column is not exerted on the cladding during PCMI. One of the reasons is the slippage between pellet and cladding in the upper portion of the fuel rod having smaller frictional forces. Another reason is the presence of axial cracks in the fuel pellets which may not allow perfect axial coupling between pellets and cladding. In addition, FRACAS-II does not model dished pellet ends. So, the calculated thermal expansion of the pellet column is larger than the actual thermal expansion. To account for these two phenomena and the modelling approximation, an empirical model based on the test data for IFA-508, Rod eleven has been developed to transmit only a portion of the axial thermal expansion of fuel to cladding during PCMI. This model is called the "slippage model." It reduces thermal expansion of the pellet column to 20% at 50 kw/m.

The transfer matrix method[8] in FRACAS-II is modified to analyze pellet and cladding coupled only axially (axial PCMI) and not radially. The transfer matrix is used to solve pseudo elastic equations at each iteration in the elastic-plastic analysis of cladding and fuel.[9]

FRACAS-II has two types of transfer matrices - one for the open gap condition and one for the radial PCMI condition. For the open gap condition, there is no coupling between pellet and cladding. Stress boundary conditions are specified at the center and outside surface of the pellet and at the inside and outside surface of the cladding. For the radial PCMI condition, there is radial and axial coupling between pellet and cladding. Stress boundary conditions are specified at the center of the pellet and outside surface of the cladding. Compatibility conditions along the radial and axial direction are specified at the pellet-cladding interface. In FRACAS-II, the generalized plane strain condition is assumed. Based on this assumption, the equilibrium equation along the axial direction is satisfied and axial stresses are calculated.

An additional PCMI model has been added to FRACAS-II to analyze an axial PCMI initiated at a lower power than radial PCMI. For the axial PCMI condition, there is only axial coupling between pellet and cladding. So in addition to the stress boundary condition at the center of the pellet and outside of the cladding, a radial stress boundary condition and compatibility condition along the axial direction at the interface should be satisfied. The axial stresses are calculated as before. The transfer matrix method for axial PCMI is described next.

2.1.1 Transfer Matrix Solution for Axial PCMI

Figure 2 shows the radial nodalization of cladding and cracked pellet This nodalization is used in deriving the transfer matrix for axial PCMI. During axial PCMI, cracked pellet and cladding are subjected to the following six conditions:

at the pellet center

$$\sigma_r(M_2) = \sigma_\theta(M_2), \tag{1}$$

at the outside surface of the pellet

$$\sigma_r(M_4\text{-}1) = -PG, \tag{2}$$

at the inside surface of cladding

$$\sigma_r(M_4) = -PG, \tag{3}$$

at the outside surface of cladding

$$\sigma_r(M_3) = -PC, \tag{4}$$

along axial direction

$$\int \sigma_z dA = F_z, \tag{5}$$

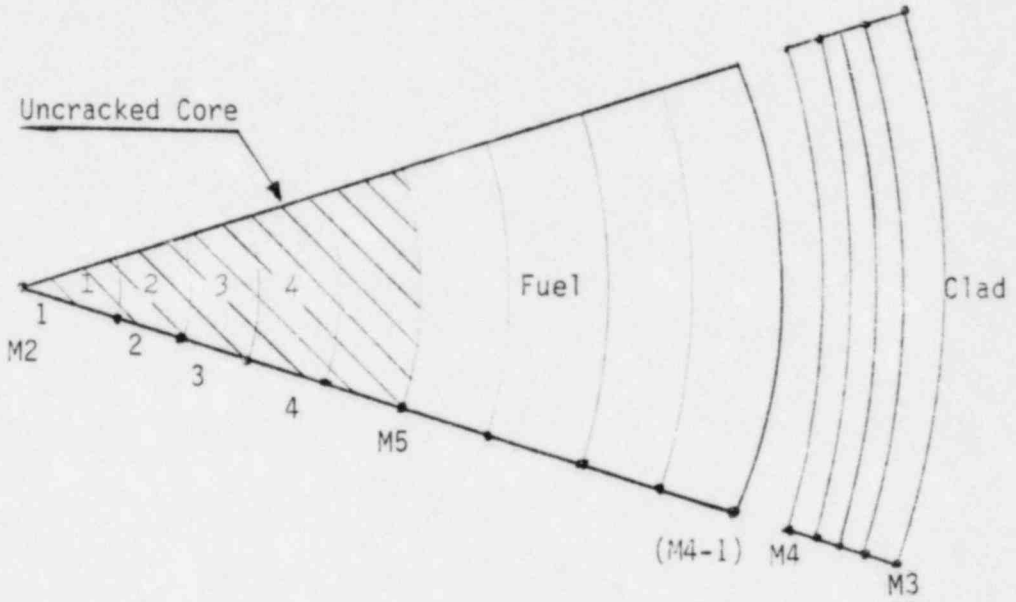

Figure 2. Nodalization of cladding and cracked pellet.

and at the pellet-cladding interface

$$\varepsilon_z(M_4) = \varepsilon_z(M_5) - \Delta\varepsilon_z, \tag{6}$$

where

σ_r, σ_θ, σ_z = radial, circumferential and axial stress (N/m^2)

PG, PC = gas pressure and coolant pressure (N/m^2)

F_z = resultant axial force (N)

ε_z = axial strain (m/m)

$\Delta\varepsilon_z$ = difference between axial strains of pellet and cladding at the instant axial PCMI begins (m/m).

Let [LP] be the transfer matrix for the cracked pellet. Then,

$$\{\sigma\}_{M_s} = [LP]\{\sigma\}_{M_2} + \{MP\} \tag{7}$$

where

$$\{\sigma\} = \begin{Bmatrix} \sigma_r \\ \sigma_\theta \\ \sigma_z \end{Bmatrix} .$$

The transfer matrix [LP] is a function of geometry and material properties, while the vector $\{M^D\}$ is a function of thermal strains and inelastic strains in addition to the geometry and material properties. As there is no radial PCMI, the radial stress at the outside surface of the uncracked pellet is equal to gas pressure, i.e.,

$$\sigma_r(M_5) = \sigma_r(M_{4\text{-}1}) = -PG. \tag{8}$$

With the aid of Equations (1) and (8), Equation (7) gives

$$\sigma_r(M_5) = LP(1,1)\sigma_r(M_2) + LP(1,2)\,\sigma_\theta(M_2) + LP(1,3)\sigma_z(M_2) + MP(1)$$

or

$$-PG = [LP(1,1) + LP(1,2)]\,\sigma_r(M_2) + LP(1,3)\,\sigma_z(M_2) + MP(1)$$

or

$$\sigma_r(M_2) = -\frac{LP(1,3)}{[LP(1,1) + LP(1,2)]}\,\sigma_z(M_2) - \frac{[MP(1) + PG]}{[LP(1,1) + LP(1,2)]}$$

$$= A_1\sigma_z(M_2) + B_1 \qquad (9)$$

where

$$A_1 = -\frac{LP(1,3)}{[LP(1,1) + LP(1,2)]}$$

$$B_1 = -\frac{[MP(1) + PG]}{[LP(1,1) + LP(1,2)]}\,.$$

Similarly, from Equation (7)

$$\sigma_\theta(M_5) = A_2\,\sigma_z(M_2) + B_2 \qquad (10)$$

where

$$A_2 = A_1\{LP(2,1) + LP(2,2)\} + LP(2,3)$$

$$B_2 = B_1\{LP(2,1) + LP(2,2)\} + MP(2)$$

and

$$\sigma_z(M_5) = A_3\sigma_z(M_2) + B_3 \tag{11}$$

where

$$A_3 = A_1[LP(3,1) + LP(3,2)] + LP(3,3)$$

$$B_3 = B_1[LP(3,1) + LP(3,2)] + MP(3).$$

Substitution of stress-strain relations in the compatibility condition, Equation (6) gives

$$\frac{1}{E(M_4)} \{\sigma_z(M_4) - V(M_4)\,[\sigma_r(M_4) + \sigma_\theta(M_4)]$$

$$+ \alpha_z T(M_4) + \varepsilon_z^p(M_4) + d\,\varepsilon_z^p(M_4)$$

$$= \frac{1}{E(M_5)} \{\sigma_z(M_5) - V(M_5)\,[\sigma_r(M_5) + \sigma_\theta(M_5)]\}$$

$$+ \alpha_z T(M_5) + \varepsilon_z^p(M_5) + d\,\varepsilon_z^p(M_5) - \Delta\varepsilon_z$$

or

$$\sigma_z(M_4) = LPC(3,1)\,\sigma_r(M_4) + LPC(3,2)\,\sigma_\theta(M_4)$$

$$+ LPC(3,3)\,\sigma_z(M_4) + MPC(3) \tag{12}$$

where

$$LPC(3,1) = \frac{V(M_4)}{E(M_4)}$$

$$LPC(3,2) = \frac{V(M_5)}{E(M_5)}$$

$$LPC(3,3) = \frac{E(M_4)}{E(M_5)}\,[A_3 - V(M_5)\,A_2]$$

$$MPC(3) = \frac{E(M_4)}{E(M_5)} [B_3 + V(M_5)\ PG - V(M_5)B_2]$$

$$+ E(M_4)\ [\alpha_z T(M_5) + \varepsilon_z^p(M_5) + d\ \varepsilon_z^p(M_4) - \Delta\varepsilon_z - \alpha_z T(M_4) - \varepsilon_z^p(M_4)$$

$$- d\ \varepsilon_z^p\ (M_4)]$$

E,V = elastic modulus (N/m^2) and Poisson's ratio, respectively

ε_z^p = inelastic strain (m/m)

$d\varepsilon_z^p$ = increment in inelastic strain (m/m).

The stress vector at node M_4 may be expressed as follows:

$$\begin{bmatrix} \sigma_r \\ \sigma_\theta \\ \sigma_z \end{bmatrix}_{M_4} = \begin{bmatrix} 1 & 0 & 0 \\ 0 & 1 & 0 \\ LPC(3,2) & LPC(3,2) & LPC(3,3) \end{bmatrix} \begin{bmatrix} \sigma_r \\ \sigma_\theta \\ --- \\ \sigma_z \end{bmatrix}_{\substack{M_4 \\ M_2}} + \begin{bmatrix} 0 \\ 0 \\ \\ MPC(3) \end{bmatrix}$$

or

$$\{\sigma\}_{M_4} = [LPC] \begin{Bmatrix} \sigma_r \\ \sigma_\theta \\ --- \\ \sigma_z \end{Bmatrix}_{\substack{M_4 \\ M_2}} + \{MPC\} \qquad (13)$$

where

$$\begin{bmatrix} \sigma_r \\ \sigma_\theta \\ --- \\ \sigma_z \end{bmatrix}_{M_2}^{M_4} = \begin{bmatrix} \sigma_r\ (M_4) \\ \sigma_\theta\ (M_4) \\ \sigma_z\ (M_2) \end{bmatrix}$$

Let [LC] be the transfer matrix for cladding. Then

$$\{\sigma\}_{M_3} = [LC]\ \{\sigma\}_{M_4} + \{MC\}\ . \tag{14}$$

The transfer matrix [LC] is a function of cladding geometry and its material properties, while the vector {MC} is a function of thermal and inelastic strains in addition to the cladding geometry and its material properties. Substitution of Equation (13) into Equation (14) gives

$$\{\sigma\}_{M_3} = [LC]\ [LPC] \left\{ \begin{matrix} \sigma_r \\ \sigma_\theta \\ --- \\ \sigma_z \end{matrix} \right\}_{M_2}^{M_4} + [LC]\ \{MPC\} + \{MC\}$$

or

$$\{\sigma\}_{M_3} = [LLC] \left\{ \begin{matrix} \sigma_r \\ \sigma_\theta \\ --- \\ \sigma_z \end{matrix} \right\}_{M_2}^{M_4} + [MMC] \tag{15}$$

where

$$[LLC] = [LC]\,[LPC]$$

$$[MMC] = [LC]\,\{MPC\} + \{MC\}.$$

Equation (15) and the boundary condition, Equations (3) through (5), are solved to calculate the hoop stress, $\sigma_\theta(M_4)$, at the inside surface of the cladding and the axial stress at the pellet center, $\sigma_z(M_2)$. Then with the aid of transfer matrices for cladding, stresses are calculated at all the cladding nodes. Equation (9) is used to calculate the radial stresses at the pellet center. Then with the aid of transfer matrices for the pellet, stresses are calculated at the pellet nodes.

2.2 Trapped-Stack Model

The mechanical interaction between pellet and cladding causes the trapping of the lower portion of the pellet column between the bottom of the cladding tube and the lowest pellet experiencing PCMI. A mechanistic model to analyze the trapped-stack configuration is presented here.

The existence of the trapped-stack configuration is due to the nonuniform axial power profile of the fuel rod. Generally, the axial power profile is of chopped cosine shape and has a peak somewhere near the middle of the rod as shown in Figure 3. The pellets near the peak of the axial power profile experience axial PCMI at a lower power than the other pellets and trap the stack of pellets in the lower portion of the rod. If the axial power profile is uniform, then all the pellets experience axial PCMI at approximately the same power and the trapped-stack configuration does not exist. In the development of the trapped-stack model, an idealized trapped-stack condition representing only one trapped stack in the lower portion of the fuel rod is assumed.

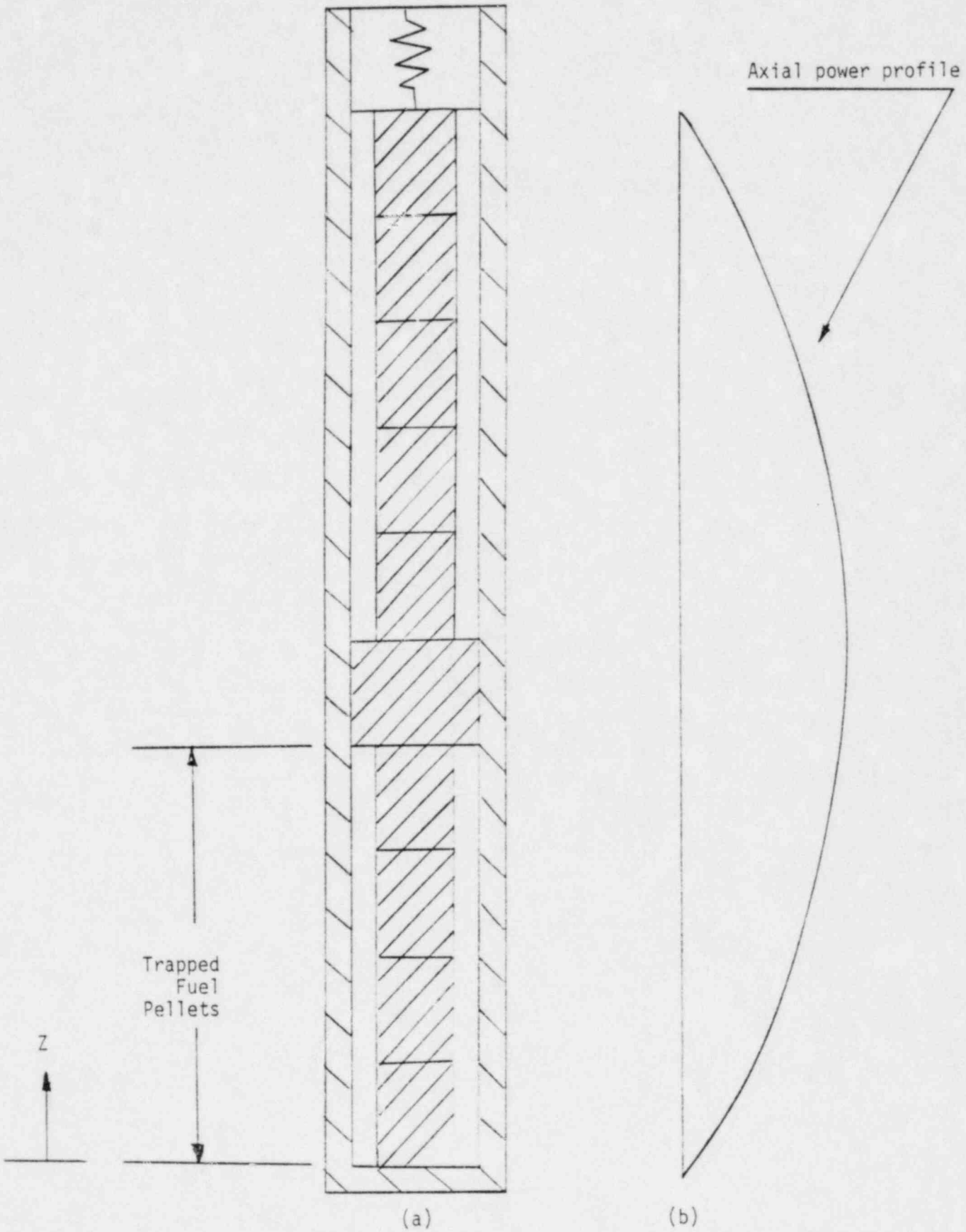

Figure 3. Trapped-stack configuration.

2.2.1 Analysis of Trapped-Stack Model

Once the stack of the pellets gets trapped between the bottom of the cladding tube and the lowest pellet experiencing axial PCMI, the trapped stack and the corresponding length of cladding tube will experience the same change in axial length. As the temperature and thermal expansion coefficient for the fuel are higher than that of the cladding, pellets in the trapped-fuel stack will experience compressive stress and the associated cladding will experience tensile stress. The constraint of equal change in the axial length of the trapped fuel stack and the corresponding cladding section, taking into account the slippage between tehm, is called the compatibility condition. This condition is satisfied as follows.

The fuel and cladding have time independent and time dependent deformations. The compatibility condition for the time independent deformations is derived here. The time independent deformations include elastic deformation of pellet and elastic-plastic deformation of cladding. So, the pellet deformation along axial direction is linear and this fact is taken into account while satisfying the compatibility condition.

Let there be n axial nodes in the trapped stack.[10] The stress-strain relations for cladding along the axial direction are as follows. For the i-th axial node in the stack, for a given time step

$$\varepsilon_z(i) = \frac{1}{E(i)} [\sigma_z - V(i) (\sigma_\theta(i) + \sigma_r(i))]$$

$$+ \varepsilon_z^p (i) + d\,\varepsilon_z^p (i) + \int_{T_o(i)}^{T(i)} \alpha_z(i)\, dT \qquad (16)$$

where

ε_z = total axial strain (m/m)

ε_z^p = axial plastic strain at the beginning of the current time step (m/m)

$d\varepsilon_z^p$ = increment in axial plastic strain during the current time step (m/m)

E,V = elastic modulus (N/m^2) and Poisson's ratio, respectively

$\sigma_r = -0.5(PG + PC)$

$$\sigma_\theta = \frac{PG\ r_i - PC\ r_o}{r_o - r_i}$$

σ_z = axial stress (N/m^2)

PG, PC = gas and coolant pressure N/m^2.

Note that in Equation (16), the axial stress σ_z is independent of the axial node, i. The axial stress σ_z may be given as

$$\sigma_z = \sigma_{z,o} + \sigma_{z,1} \tag{17}$$

where

$\sigma_{z,o}$ = axial stress in cladding at the beginning of the time step

$\sigma_{z,1}$ = change in axial stress in cladding due to trapped stack condition during current time step.

The stress $\sigma_{z,o}$ consists of axial stresses due to pressure loads and the stresses due to trapped-stack conditions in the previous time steps. The stress $\sigma_{z,1}$ is an increment in the stresses due to trapped-stack condition during the current time step.

The compatibility condition is

$$\Delta\ell = \sum_{i=1}^{n} [\varepsilon_z(i) - \varepsilon_{z,o}^{(i)}]\, dz(i) + \frac{\sigma_{z,1}(A_c/A_f)}{K_{feq}} \tag{18}$$

where

$\Delta\ell = \Delta\ell_f - \Delta\ell_c$

$\Delta\ell_f$ = free thermal expansion of pellet column during the time step (m)

$\Delta\ell_c$ = free thermal expansion of trapped cladding length during the time step (m)

$\varepsilon_{z,o}$ = total axial strain at the beginning of time step (m/m)

dz = length of an axial node (m)

A_c, A_f = effective cross-sectional area of cladding and fuel respectively (m^2)

K_{feq} = axial stiffness of pellet column (stress/unit deflection) (N/m^3).

In the calculation of free thermal expansions $\Delta\ell_f$ and $\Delta\ell_c$, the trapped column and associated cladding length are subjected to the thermal and pressure loads of the current time step and the trapped stresses present at the end of the previous time step. The two terms on the right hand side of Equation (18) are the changes in the trapped cladding and pellet column lengths, respectively, during the time step due to trapped-stack condition. Substitution of Equations (16) and (17) into Equation (18) gives

$$\left[\sum_{i=1}^{n} \frac{dz(i)}{E(i)} + \frac{(Ac/A_f)}{K_{feg}}\right] \sigma_{z,1} = \Delta\ell - \sum_{i=1}^{n} \left[\frac{1}{E(i)} \{\sigma_{z,o} - V(i)(\sigma_\theta(i) + \sigma_r(i))\} + \varepsilon^p_{z,o}(i) + d\,\varepsilon^p_z(i) + \int_{T_o(i)}^{T(i)} \alpha_z(i)\, dT - \varepsilon_{z,o}(i)\right] dz(i). \quad (19)$$

Equation (19) and the modified Prandtl-Reuss equation are solved to calculate the stress $\sigma_{z,1}$, the increment in the trapped stresses. The modified Prandtl-Reuss equation is

$$d\,\varepsilon_z^p = \frac{d\varepsilon_p}{3\,\varepsilon_{et}} (2\varepsilon_z' - \varepsilon_x' - \varepsilon_y') \qquad (20)$$

where

$d\varepsilon_p$ = equivalent plastic strain increment

ε_x', ε_y', ε_z' = modified total strains

ε_{et} = equivalent modified total strain.

Equations (19) and (20) are solved iteratively.

As the reactor power is increased from zero, first axial PCMI takes place near the peak of the axial power profile, and the trapped-stack configuration begins. As the reactor power increases further, additional axial nodes experience PCMI, and the length of the trapped stack reduces. The trapped stresses at the axial nodes which were previously in the trapped-stack condition, should be included in the PCMI analyses. The trapped stresses at an axial node will be released when that node is no longer in the trapped-stack configuration and is not experiencing any PCMI.

Figure 4 presents five different states of the trapped-stack configuration. Figure 4-a shows the beginning of the trapped stack. The lowest PCMI has taken place at the sixth axial node, so the trapped stack consists of five axial nodes. The trapped stresses (stresses due to trapped-stack configuration) in the cladding and pellet column are T_1 (tensile) and C_1 (compressive), respectively. As the reactor power increases further, axial nodes 4 and 5 experience PCMI and the trapped-stack length reduces and

consists of three axial nodes (Figures 4-b). The trapped stresses in the cladding and pellet column of the shortened trapped stack are increased to T_2 (tensile) and C_2 (compressive), respectively. The trapped stresses T_1 and C_1 at axial nodes 4 and 5 are included in the PCMI analysis. Figures 4-c, 4-d, and 4-e represent the trapped stack configurations while the stack length is increasing and are discussed in the next section.

2.2.2 Equilibrium Condition During Increasing Trapped-Stack Length

As the reactor power is decreased, the length of the trapped stack will increase and finally, when the reactor power is low enough, the trapped-stack configuration will not exist. As the length of the trapped stack increases, the magnitude of the trapped stresses will reduce. At time t, when the length of the trapped stack is increased, the axial stresses at node 4 just added in the trapped stack are different than those at nodes already present in the trapped stack. So at time t, an axial equilibrium condition should be satisfied such that all the axial nodes in the longer trapped stack have the same axial stresses.

Figures 4-b to 4-e illustrate the trapped stack configurations during decreasing rod power. At time t, the PCMI at node 4 is released and the trapped-stack length is increased from three axial zones (Figure 4-b) to four axial zones as shown in Figure 4-c. At time t, when the increase in the trapped-stack length takes place, the axial stresses at the first three nodes are T_2 and C_2 and at node 4 they are T_1 and C_1. Figure 4-d represents the trapped stack configuration at time t after axial equilibrium is satisfied and the trapped stresses at the first four nodes are the same and equal to T_3 and C_3. As the rod power decreases further, the remaining locked nodes are released and the trapped stresses are reduced to zero (Figure 4-e). The axial stresses (T_3, C_3) satisfying the equilibrium may be calculated as follows:

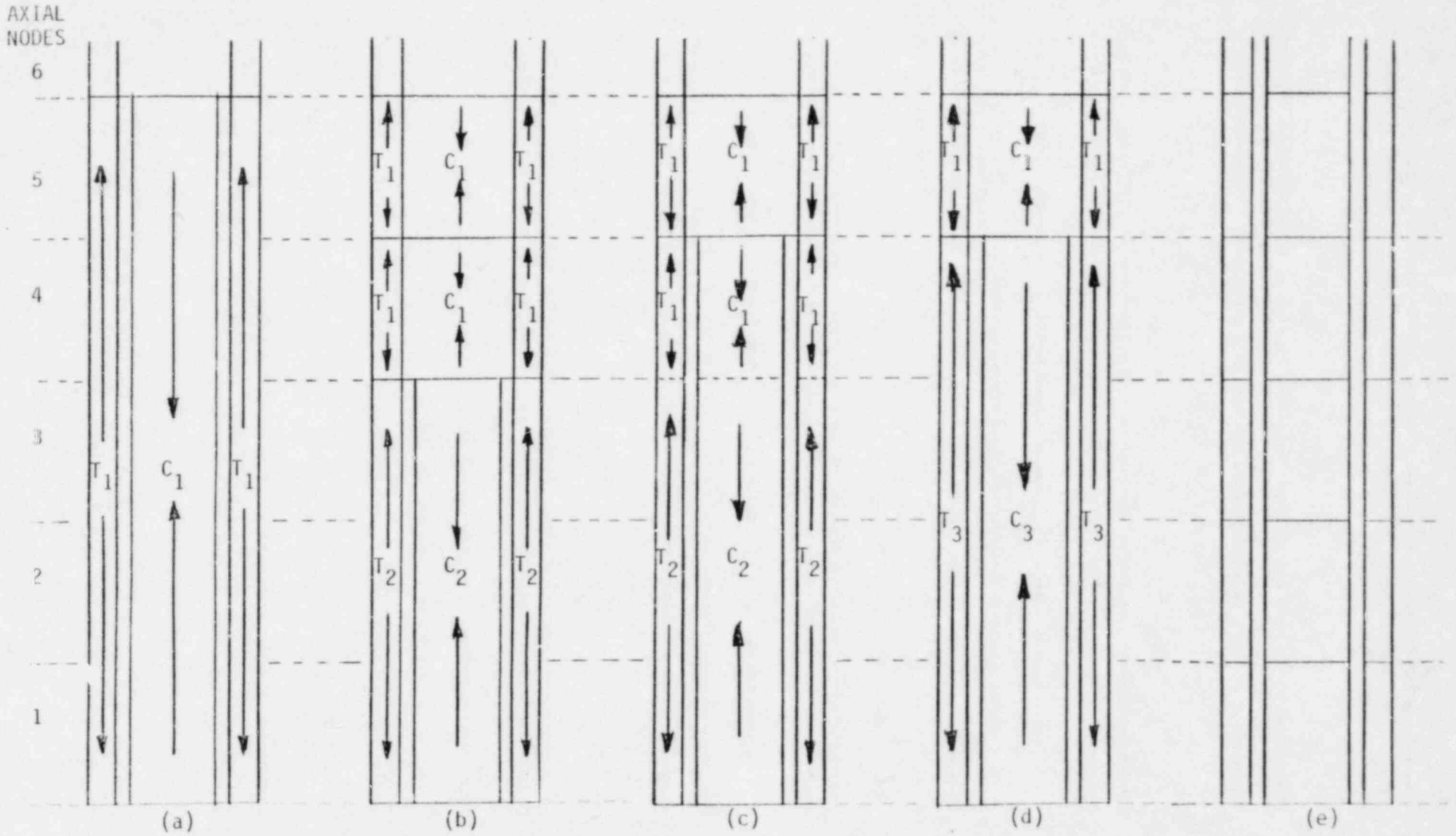

Figure 4. Five different states of trapped stack configurations: (a) Initiation of trapped stack condition, (b) Shortened trapped stack, (c) Extended trapped stack - before equilibrium is satisfied, (d) Extended trapped stack - after equilibrium is satisfied, and (e) Trapped stack condition is released.

The elastic-plastic stress-strain relation along the axial direction at the trapped node i, is

$$\varepsilon_z(i) = \frac{1}{E(i)} \left[\sigma_z - V(i)\left\{\sigma_\theta(i) + \sigma_r(i)\right\}\right] \tag{21}$$

$$+ \varepsilon_z^p(i) + d\,\varepsilon_z^p(i)$$

where

σ_z = axial stress in trapped length of cladding

$$= \sigma_{z,t} + \sigma_{z,p} \tag{22}$$

$\sigma_{z,t}$ = trapped stresses

$\sigma_{z,p}$ = stresses due to pressure loading.

While satisfying the equilibrium condition at time t, the cladding and the pellet column lengths in the trapped stack will change. These two length changes are equal. Let ΔL_c and ΔL_f be the changes in the length of the trapped cladding and pellet column, respectively. Then

$$\Delta L_c = \sum_{i=1}^{n} \left[\varepsilon_{z(i)} - \varepsilon_{z,o}(i)\right] dz(i) \tag{23}$$

where $\varepsilon_{z,o}$ is the axial strain in cladding just before equilibrium is satisfied,

and

$$\Delta L_f = DELF(o) - DELF(1) \tag{24}$$

where

DELF(o) = change in the length of the pellet column due to trapped stresses just before equilibrium is satisfied

DELF(1) = change in the length of the pellet column due to trapped stresses just after equilibrium is satisfied

$$= \frac{\sigma_{z,t}(Ac/Af)}{K_{feq}} \quad . \tag{25}$$

To satisfy compatibility,

$$\Delta L_c = \Delta L_f \tag{26}$$

Equations (21) through (25) are substituted in Equation (26), and then Equation (20) and (26) are solved to determine the trapped stress, $\sigma_{z,t}$.

2.3 Relocation Model

The fuel relocation model is a function of burnup, power, and initial gap size. The correlation developed by Shimada and Oguma [5] is used. Shimada and Oguma found that a reasonable correlation exists between fuel relocation and the number of cracks in a pellet. They also assumed that the dependence of relocation on power and burnup is similar to that of the number of cracks. The number of cracks in a pellet increases rapidly with increasing burnup until about 5.0 MWd/KgUO_2 after which the number of cracks remain constant. Below 5.0 MWd/KgUO_2, the number of cracks in a pellet is directly proportional to power from 10 kW/m to 40 kW/m and constant above that.

The correlation presented in Reference 5 (modified for SI units) is

$$R_e = G_o[0.4 + (0.01\ P - 0.3)e^{aBu}] + (0.6\ G_o - A)\ (1 - e^{bBu}) \qquad (27)$$

where

R_e = relocation (m)

G_o = initial fuel-cladding gap (m)

P = linear heat rate (kW/m)

Bu = burnup (MWs/kgU)

a, b, A = experimental constants.

The authors determined the empirical constants using experimental data from two Halden tests, IFA-211 and IFA-410. The constants are $A = 6.5 \times 10^{-5}$, $a = -2.5463 \times 10^{-5}$ and $b = -0.9576 \times 10^{-6}$. This model is used to calculate relocation strain for the FRAP-T6 code until PCMI occurs. The fuel relocation then remains constant.

3. MODEL USE AND IMPLEMENTATION

The advanced models for fuel rod deformation are incorporated in FRACAS-II and FRAP-T6. The use of these models and their implementation in FRAP-T6 is described here. The early axial PCMI model is discussed first, then the trapped stack model, and finally the fuel relocation model is discussed.

3.1 Early Axial PCMI Model - Use and Implementation

This model initiates axial PCMI at power lower than that required to initiate radial PCMI. This model assumes that axial PCMI begins when the radial gap between cladding and fuel is less than the locking gap. The magnitude of the locking gap is an input to FRAP-T6 and is specified as a fraction of the cold gap. The default value for the locking gap is zero. The magnitude of the locking gap may be determined from experimental results or from detailed analysis of the fuel rod. The first two acceptance tests illustrate the calculation of the locking gap from the test results for small and large gap rods. For IFA-508, Rod 11, the magnitude of the locking gap is 0.02 mm.

A parameter IGAP describing the status of the structural gap at each axial node is defined in FCMI2. When strucutural gap is greater than locking gap, IGAP is set equal to zero and TRANSF performs an open gap (uncoupled) analysis. When the structural gap is positive and less than locking gap, IGAP is set equal to one and TRANSF performs an axially coupled analysis (axial PCMI). When the structural gap is zero, IGAP is set equal to two, and TRANSF performs an axially and radially coupled analysis (axial and radial PCMI).

3.2 Trapped-Stack Model - Use and Implementation

The mechanical interaction between pellet and cladding causes trapping of the lower portion of the pellet column between the bottom of the cladding tube and the lowest pellet experiencing PCMI. The computer logic to analyze the trapped-stack configuration is presented in the flow diagrams

shown in Figures 5 and 6.

The flow diagram in Figure 5 shows the overall logic in FCMI2 used to analyze the trapped-stack condition. If the trapped stack condition is present in the previous time step, then FCMI2 determines whether or not the length of the trapped stack is changed during the current time step. If the length is not changed, then STACK2 is called to analyze the trapped-stack condition for the complete time step. If the length is changed, then STACK2 is called two times to analyze the old and new trapped stack conditions.

FRACAS-II analyzes two types of mechanical interactions between cladding and pellets: PCMI and trapped-stack condition. In PCMI analysis, there is no coupling between two axial nodes and the pellet and cladding are modeled with a number of radial nodes at each axial node. In trapped stack analysis, the gap between cladding and pellet is greater than the locking gap and axial nodes are coupled with each other. So in trapped stack analysis, each axial zone in fuel and cladding is represented by only one node. When STACK2 is called from FCMI2, average values of stresses and strains at each axial node are passed through the common blocks.

The flow diagram in Figure 6 shows the overall logic in STACK2. First the differential free thermal expansion for the trapped stack is calculated. This differential expansion is the forcing function to analyze the trapped stack. Then the stiffness of the pellet column is calculated. Finally COMPAT is called to solve the elastic-plastic equations along the axial direction. COMPAT calculates trapped stresses in the trapped stack. At the end of the time step, each axial node in the trapped stack is analyzed to determine the magnitude of the structural gap. Trapped stresses are included in this analysis.

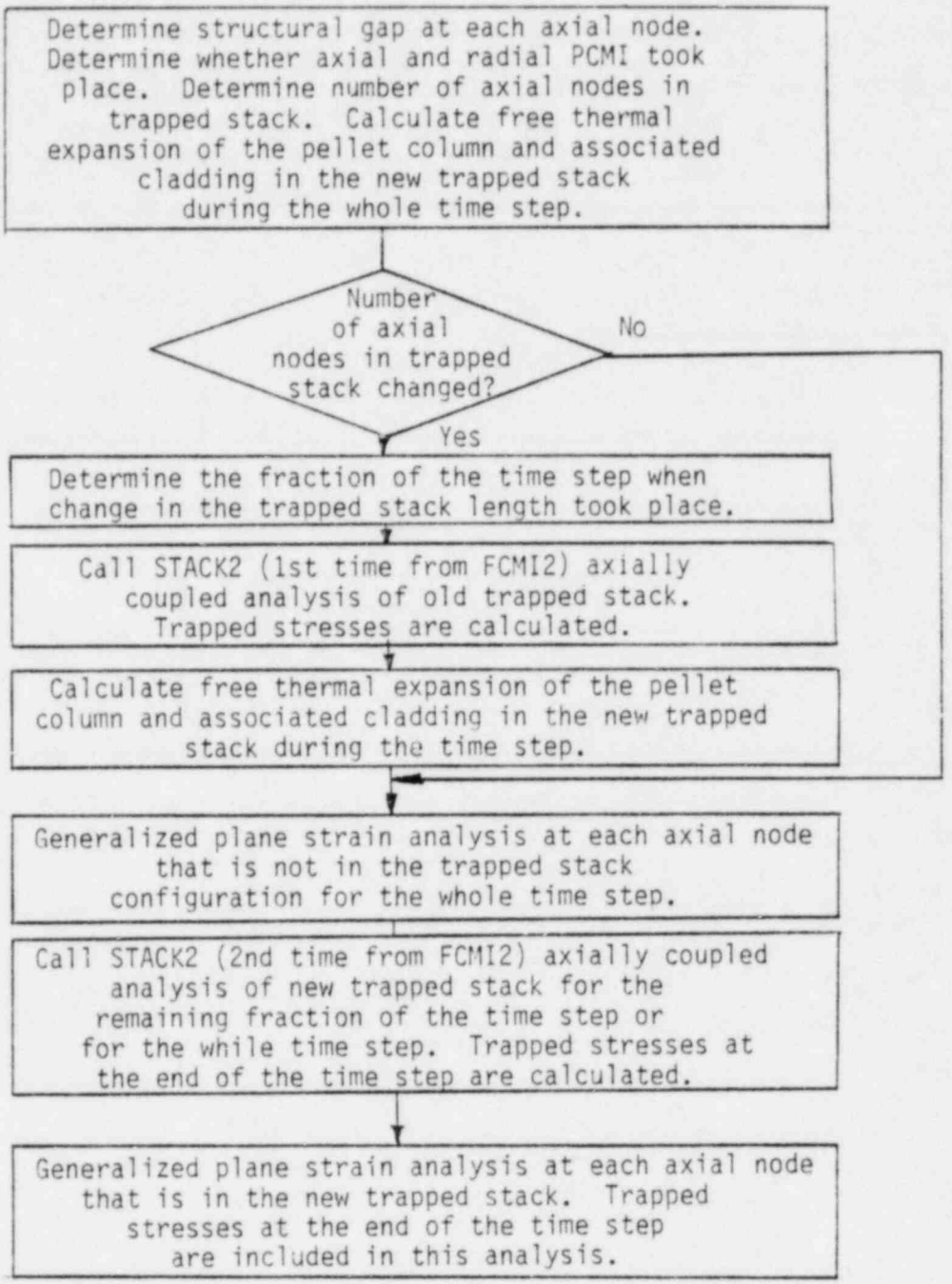

Figure 5. Flow diagram for subroutine FCMI2.

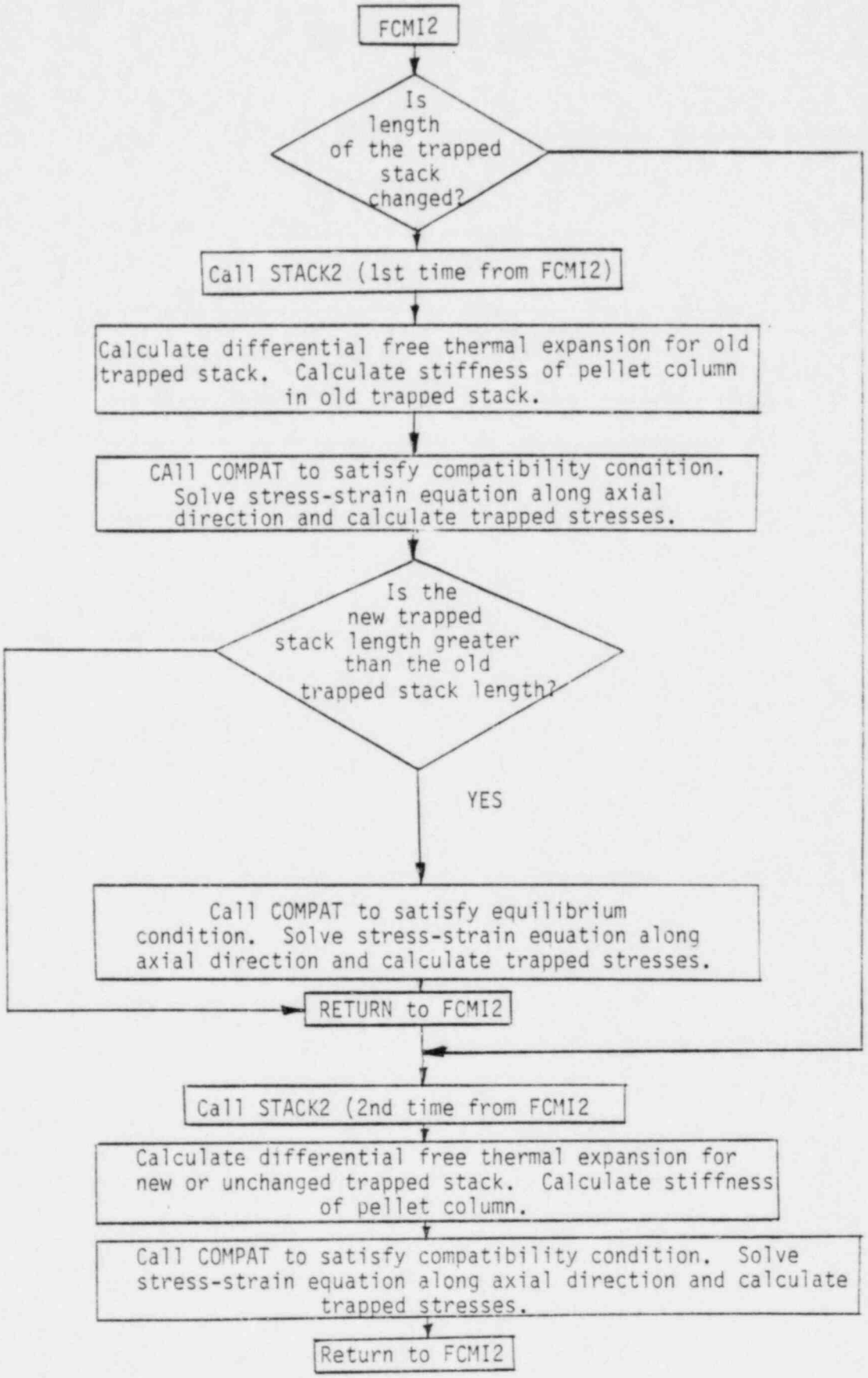

Figure 6. Flow diagram for logic in STACK2.

3.3 Relocation Model - Use and Implementation

In order to implement this model into FRAP-T6, five things were done. First, the previous relocation strain, RELOCO, is initialized either from a FRAPCON-2 restart in subroutine RESTFS or is set to zero in subroutine INIFC2. The second step was to remove the previous relocation model. The third step was to calculate the relocation strain, FVFRO, for each axial and radial node in subroutine DEFRM2 once for each timestep (when ITCNT and ITCNTD equal 1) using Equation 27. The fourth step was to update the previous relocation strain value, RELOCO when NRELAX is equal to 1. Finally, the relocation strain is loaded into the strain arrays to be used by the FRACAS-II subcode.

Strain associated with relocation is now used by FRACAS-II instead of the previous treatment of increasing the pellet radius.

3.4 Computer Coding of Models

Tables 1 and 2 contain glossaries of pertinent variables associated with the addition of the trapped-fuel stack, early axial PCMI, and relocation models. A copy of the updates and the subroutines changed or added appears on the microfiche attached to the back cover.

TABLE 1. GLOSSARY OF FORTRAN VARIABLE NAMES USED IN EARLY AXIAL PCMI AND TRAPPED STACK MODELS.

FORTRAN NAME	DESCRIPTION
AEFC	Cross-sectional area of cladding (m^2)
AEFF	Cross-sectional area of the uncracked portion of pellet (m^2)
DCLDH	Total change in the length of the cladding (m)
DEFLU	Axial deflection of fuel column due to unit stress (m^3/N)
DELC	Free thermal expansion of cladding length associated with trapped pellet column (m)
DELCTF	Free thermal expansion of associated cladding length during TSTFRC fraction of time step (m)
DELF	Free thermal expansion of trapped pellet column (m)
DELFTF	Free thermal expansion of trapped pellet column during TSTFRC fraction of time step (m)
DELSTK	Differential thermal expansion during a timestep (m)
DELTH	Total change in the length of the pellet column (m)
DGAP(I)	Locking gap at axial node I (m)
ECREP2(K,N)	Effective ladding creep
EP2(K,N)	Effective lastic Strain
EPP2(K,N,L)	Plastic strain
EPS2(K,N,L)	L-th component of total strain at radial node N at end of time step of axial node K L = 1 = Hoop direction L = 2 = Axial direction L = 3 = Radial direction
EPSO2(K,N,L)	Misc. initial strains
IAGAP	= 0 No PCMI at any axial node ≠ 0 lowest axial node having a PCMI
IAGAPO	Magnitude of IAGAP parameter at the end of the previous time step
IGAP(I,1)	= 0 No PCMI at axial node I = 1 Only axial PCMI at axial node I = 2 axial and radial PCMI at axial node I

TABLE 1. (CONTINUED)

KTPSTK	No. of axial nodes in a trapped stack
N4	Convergence parameter = 0 solution is converged = 1 solution is not converged
NOLDGP(I,1)	Magnitude of IGAP(I,1) parameter at the end of the previous time step
PEP2(K,N)	Effective plastic strains at start of time step
PEPP2(K,N,L)	Plastic strains at start of time step
REPS2(K,L)	Fuel and cladding axial strain at start of fuel-cladding
RFC2(L)	Undeformed radius to radial node L (m)
SIG2(K,N,L)	Stress (N/m^2)
SIGZO(I)	Trapped axial stresses at axial node I at the end of the previous time step (N/m^2)
THKGPI(1,I)	Structural gap between fuel and cladding at the axial node I (m)
TFC2(L)	Input radial temperature distribution (k)
TSTFRC	Fraction of the time step at which length of the trapped stack is changed

TABLE 2. RELOC2 VARIABLES AND DEFINITIONS

Variable	Type	Definition	Units
RESTRN	output	relocation strain in the cracked fuel	-
BU	input	fuel burnup	MWs/kgU
GAP	input	as-fabricated radial fuel cladding gap	m
POWER	input	average local power	kW/m
RP	input	as-fabricated pellet radius	m
AA	local	experimental constant	kgU/MWs
B	local	experimental constant	kgU/MWs
A	local	experimental constant	m
RE	local	relocation	m

4. ACCEPTANCE TEST RESULTS CONCLUSIONS AND RECOMMENDATIONS

Acceptance tests were performed with FRAP-T6 after each of the new models were added to assure that the models were working properly. The cases shown for the final acceptance testing include the calculation of the initiation of axial PCMI for IFA-508 Rods 11 and 13, calculation of trapped-stack stresses, and comparison of old and new relocation strains.

4.1 Comparisons With IFA-508 Experimental Data

The purpose of this section is to present an assessment of the FRACAS-II model additions through comparison with IFA-508 experimental data. IFA-508 is an irradiation test of three experimental fuel rods (Rods 11, 12 and 13) in the Halden Boiling Water Reactor using an on-power fuel rod diameter measuring rig. Test data for Rods 11 and 13 are analyzed, and the results of these analyses are compared with the corresponding FRACAS-II calculations.

The physical dimensions and material properties of the fuel and cladding for Rods 11 and 13 are given in Table 3. The cladding material is fully annealed Zircaloy-2 tubes with autoclaving on both surfaces. The fuel consists of UO_2 pellets with 7-mm diameter dishing at both ends and sintered at 1980 K. The coolant is heavy water pressurized to 3.4 MPa at a temperature of 513 K. The fuel rods are cooled at nucleate boiling under natural circulation. During the first cycle, a stepwise power increase, as shown in Figure 7 was imposed on the fuel rods. Power was held at nominal linear heat ratings (LHR) of 30, 40 and 50 kW/m. Between these power levels, power was raised 0.3 kW/m per minute.

The coupling between the mechanical calculations and the thermal calculations is strong, therefore, a good temperature comparison between the code calculation and the experimental data must exist before the mechanical modeling can be adequately assessed. Figure 8 presents the comparison between calculated and measured centerline temperature for both Rod 11 and Rod 13 of IFA-508. This comparison is good and the following mechanical calculations will be based on a proper temperature distribution.

TABLE 3. DESCRIPTION OF IFA-508 TEST

A. Physical Dimensions

Characteristic	Value	
	Rod 11	Rod 13
Fuel Pellet O.D., (mm)	11.31	11.21
Fuel Pellet Length, (mm)	15.00	15.00
Cladding I.D., (mm)	11.41	11.43
Cladding O.D., (mm)	12.19	12.19
Fuel-Cladding Normal Gap, (mm)	0.05	0.11
Active Fuel Stack Length, (mm)	420.00	420.00

B. Material Properties

Characteristic	Value
Fuel Density (% TD)	94.9
Grain size (μm)	10.0
Burnup	0.0
Cladding Yield Strength (MPa) (at 0.2% strain)	140 at 616 K
Cladding Ultimate Tensile Strength (MPa)	240 at 616 K
Fill Gas	He at 1.013 (MPa)

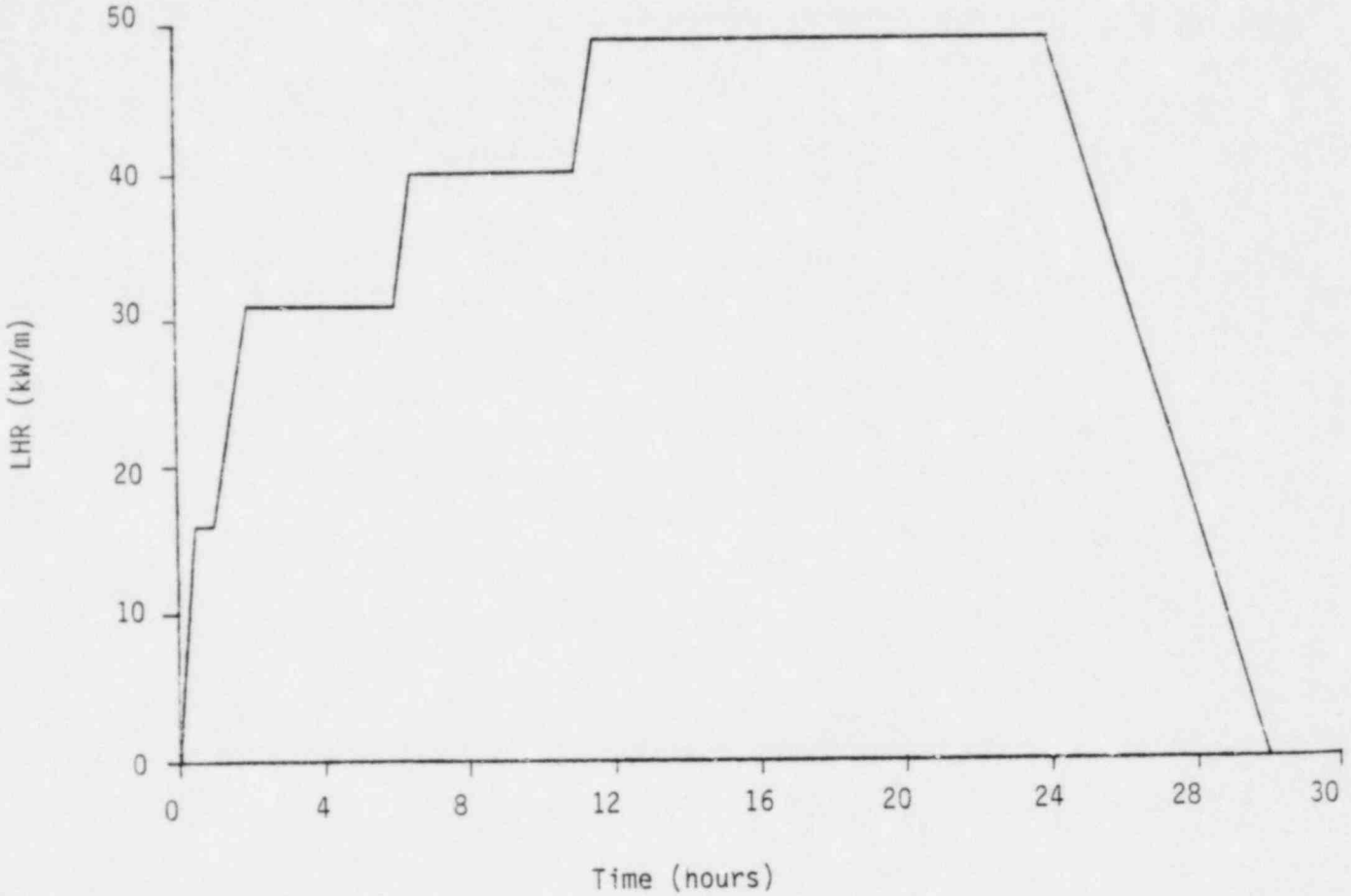

Figure 7. Stepwise power-up pattern in the initial cycle.

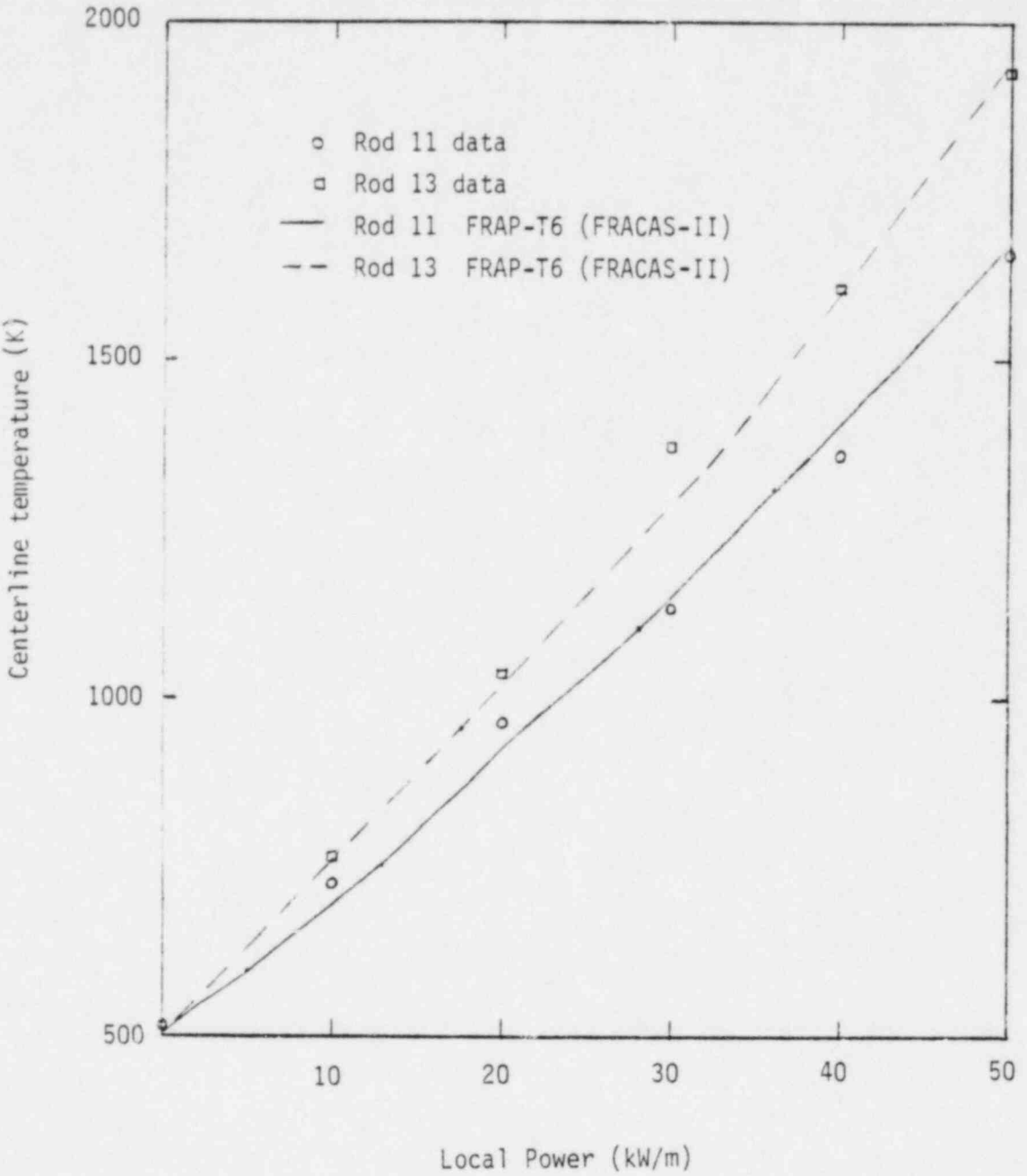

Figure 8. Calculated and measured centerline temperature versus local rod power for Rods 11 and 13 of IFA-508.

In the following, comparisons of FRAP-T6 mechanical calculations using FRACAS-II with small and large gap rods are presented. As was shown in Figure 1, axial PCMI starts at a lower power than does radial PCMI in Rod 11 of IFA-508. The axial PCMI starts at approximately 15 kW/m while radial PCMI starts at about 29 kW/m. Figure 9 shows a comparison of FRAP-T6 calculations before and after the added FRACAS-II models with IFA-508 experimental data for axial cladding strain.

The calculated power at fuel-cladding lockup for axial PCMI is 18 kW/m with the new FRACAS-II version while the previous model calculated axial PCMI at 47 kW/m. This is greatly improved and is in good agreement with the experimental data. As described in Section 3.1, an additional input is required called the "locking gap". This was determined by examining axial cladding strain versus power data to find the power at which axial PCMI occurred. The rod was then analyzed using all models with the "locking gap" set to zero. The power level at which axial PCMI should occur is examined to find the structural gap at the peak power node. This value is used as the "locking gap" for the final analysis.

Table 4 shows the relative strains at Node 4 during the early part of the IFA-508 power cycle. The axial PCMI takes place at about 21.72 kW/m to 36.09 kW/m, the axial strain in the cladding increases, causing negative hoop strain due to Poisson's effect. Therefore, the early axial PCMI model is correctly incorporated in FRAP-T6.

Table 5 shows the trapped stresses in Rod 11 during initial power cycle. The first axial PCMI takes place at Node 4 at 20.05 kW/m and it traps lower three axial nodes. The trapped stresses at Nodes 1, 2, and 3 are increased from 0.0 MPa at 18.38 kW/m to 2.6 MPa at 20.05 kW/m. As power increased from 20.05 kW/m to 21.72 kW/m, Nodes 2 and 3 experience axial PCMIs and only Node 1 remains in trapped stack configuration. At 23.39 kW/m, Node 1 experiences axial PCMI and the trapped stack configuration no longer exists. At 23.39 kW/m, the trapped stresses at Nodes 1, 2 and 3 are 18.82, 12.96 and 12.96 MPa, respectively. These trapped stresses remain constant until the axial PCMIs are released at these nodes at the end of the power cycle. Therefore the trapped stack model is correctly incorporated in FRAP-T6.

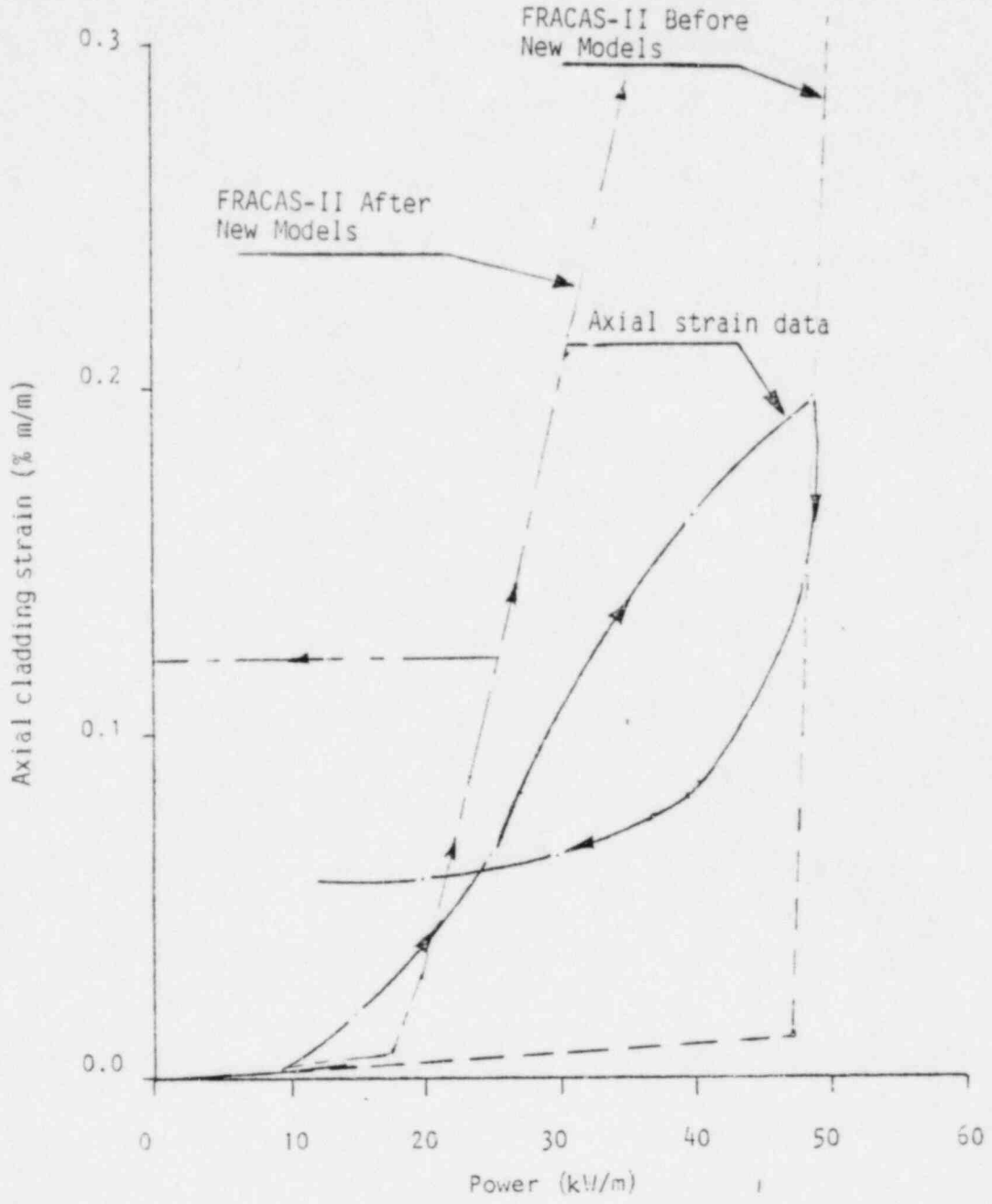

Figure 9. Calculated and measured cladding axial strains versus linear heat rating for Rod 11 during initial power cycle.

TABLE 4. STRAINS AT NODE 4 DURING EARLY PART OF POWER CYCLE

	Relative strains at node 4	
PEAK POWER	AXIAL STRAIN	HOOP STRAIN
0	0	0
18.38	.0039	.006
20.05	.0099	.005
21.72	.0349	-.004
23.39	.0599	-.013
25.06	.0859	-.022
26.73	.1129	-.031
28.40	.1399	-.041
30.08	.1669	-.051
31.75	.1949	-.061
33.42	.2239	-.071
36.09	.2579	.0255

TABLE 5. TRAPPED STRESSES IN IFA-508 ROD 11 DURING THE INITIAL POWER CYCLE.

Power, kw/m	Trapped stresses, MPa		
	Node 1	Node 2	Node 3
18.32	0	0	0
20.05	2.6	2.6	2.6
21.72	14.06	12.96	12.96
23.39	18.82	12.96	12.96
55.12	18.82	12.96	12.96
31.58	18.82	12.96	12.96
0	0	0	0

The relocation strain calculated by the burnup and power dependent relocation model was 0.00405. This differs from the previous model which calculated a constant 0.00054 relocation strain. The lower relocation strain results in radial PCMI at 45 kW/m. The current model results in radial PCMI at 35 kW/m while the experimental data indicates that radial PCMI occurred at about 30 kW/m. This is a significant improvement.

Figure 10 presents measured and calculated cladding axial strain versus linear heat rating for IFA-508 Rod 13. This was a large gap rod, however, axial PCMI occurred in it also. FRACAS-II calculated axial PCMI at 44 kW/m before the new models were added. After the new models the initiation of PCMI was calculated to be approximately 24 kW/m. The experimental data indicates PCMI at about 20 kW/m. Again this is in good agreement.

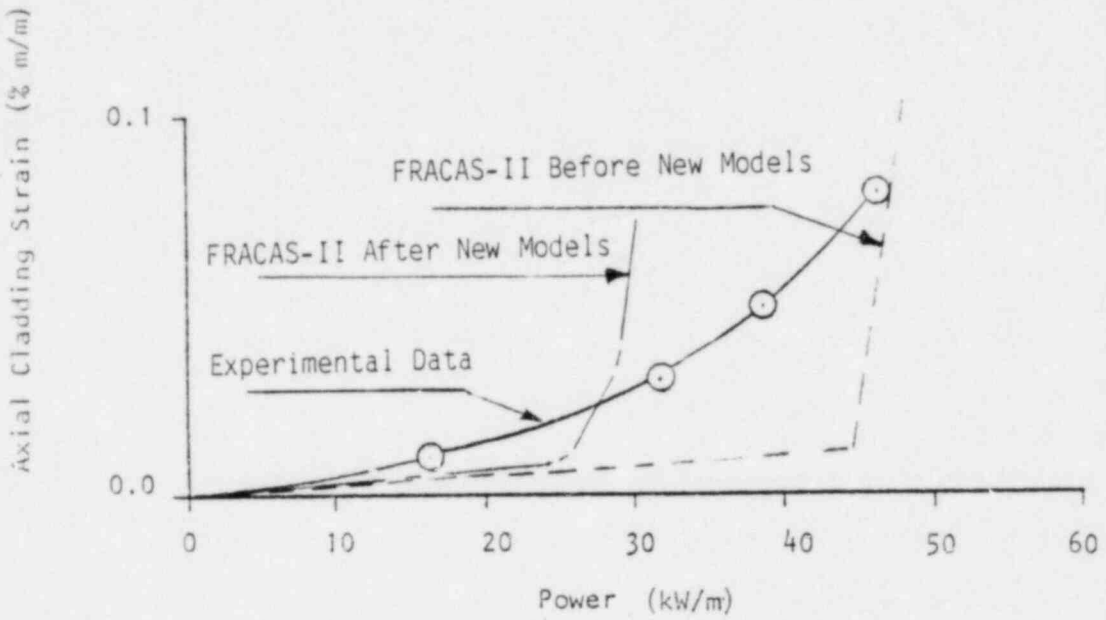

Figure 10. Measured axial cladding strain in Rod 13 versus linear heat rating during initial power cycle.

4.2 Conclusions and Recommendations

The advanced deformation models for FRAP-T6 have been tested through comparison with experimental data. The experimental data are from the IFA-508 Rod 11 and Rod 13 tests. Based on the comparisons presented in Section 4.1, it is concluded that the advanced deformation models perform as intended. FRACAS-II now calculates the initiation of axial PCMI and radial PCMI. These models eliminate the major modeling deficiencies reported in Reference 4. This conclusion is supported by the axial and hoop strains reported in Table 3 and trapped stresses reported in Table 4. However, additional models are needed to model fuel creep, fuel relocation relaxation and slippage between the fuel and cladding during PCMI. The need for additional models are supported by the following observations:

1. The analyses of IFA-508 Rod 11 and Rod 13 show that calculated cladding extension is larger than reported in the tests (see Figure 9). The discrepancies between the analytical and test results can be partially eliminated by incorporating a fuel creep model in FRAP-T6. The remaining discrepancy may be eliminated by addition of a model that allows for slippage between fuel and cladding.

2. The analyses of IFA-508 Rod 11 and Rod 13 show that calculated cladding hoop strains are larger than reported in the tests. The discrepancy between the analytical and tests results can be partially eliminated by addition of a fuel relocation relaxation model.

The results of this development activity have shown that four changes need to be made to FRACAS-II to complete the package of basic phenomena which should be modeled. The first two changes are to add models which are currently developed and ready to incorporate into FRAP-T6 (fuel creep and relocation relaxation). The third is to use experimental data to develop an empirical correlation to model the phenomena which has been attributed to fuel-cladding slippage. The final change is to examine and adjust constants in the new fuel relocation model to account for the influence

of the host code, FRAP-T6.

The modeling deficiencies identified in the FRACAS-II developmental assessment report are eliminated by addition of the advanced deformation models presented in this report. The need for the fuel creep, relocation relaxation, and slippage models has been identified. It is expected that incorporation of these additional models would complete the development of the FRACAS-II subcode and provide good comparison between FRAP-T6 stress-strain calculations and experimental data. As a result, the FRACAS-II model should reliably determine the extent of cladding damage and ultimately cladding failure.

5. REFERENCES

1. G. A. Berna et al., FRAPCON-2: A Computer Code for the Calculation for Steady State Thermal-Mechanical Behavior of Oxide Fuel Rods, NUREG/CR-1845, December 1980.

2. L. J. Siefken et al., FRAP-T6: A Computer Code for the Transient Analysis of Oxide Fuel Rods, EGG-CDAP-5410, April 1981.

3. Bohn, M. P., FRACAS-II: A Subcode for the Mechanical Analysis of Nuclear Reactor Fuel Rods, CDAP-TR-78-038, September 1978.

4. V. N. Shah, Developmental Assessment of FRACAS-II, EGG-CDAP-5411, May 1981.

5. Shimade, S. and Oguma, M., Analysis of Fuel Relocation Using In-Pile Data from IFA-211 and IFA-410, Enlarged Halden Programme Group Meeting on Fuel Performance Experiments and Evaluation, Volume III, HPR-229, August 1979.

6. Hoope, N., Improvements to COMETHE III-J Fuel Rod Modeling Code, Fuel Element Performance Computer Modeling Conference, Blackpool, U. K., March 1978.

7. Wiesenack, W., Analysis of Early Axial Interaction with the Fuel Modelling Program MARS, OCED Halden Reactor Project, HWR-327.

8. Pestel, E. C. and Leckie, F. A., Matrix Methods in Elastomechanics, McGraw-Hill, 1963.

9. Mendelson, A. Plasticity: Theory and Application, MacMillan, 1968, pp. 204-208.

10. Bohn, M. P., FRACAS - A Subcode for the Analysis of Fuel Pellet-Cladding Mechanical Interaction, TREE-NUREG-1028, April 1977, pp. 38-41.